

Spacecraft Formation Optimization with a Multi-Impulse Design

Aaron B. Hoskins* and Ella M. Atkins†
 University of Maryland, College Park, MD 20742

Satellite formation flight has emerged as a method to increase science return and enable missions that had been impossible with a single spacecraft. Formations often must maintain a precise geometry, complicating mission design given natural orbit dynamics. This paper presents a multi-impulse formation design strategy that is a compromise between active control and drift solutions. This design formulation is applied to optimize the Magnetospheric Multi-scale tetrahedron mission using two optimization algorithms, a hierarchical strategy and a particle swarm approach. Results are presented for a variety of multi-impulse problem specifications, demonstrating that a multi-impulse solution is a viable strategy that can dramatically improve formation accuracy and longevity at minimal fuel cost.

Nomenclature

\mathbf{v}	= velocity of a particle for the particle swarm optimization algorithm
\mathbf{x}	= position of a particle for the particle swarm optimization algorithm
\mathbf{g}_{best}	= vector location and cost of best candidate solution so far investigated by any particle
$\mathbf{p}_{\text{best},i}$	= vector location and cost of best candidate solution so far investigated by a specific particle
ω	= inertial weight factor used to determine influence of current state on next state
c	= constant coefficient to determine weight of cognitive (c_1) and social (c_2) influence
r	= random number to vary search
Δt	= time step
\mathbf{T}	= target frame. It is the reference orbit for the formation
\mathbf{V}	= vehicle frame. It is a frame that is offset from the \mathbf{T} -frame
$(a, e, i, \tilde{\omega}_{\text{true}})$	= orbital elements of \mathbf{T} -frame
(V_x, V_y, V_z)	= offsets from \mathbf{T} -frame that define origin of \mathbf{V} -frame
Δv	= angle between burn application sites
v_c	= angle from perigee to center of Δv
v_p	= angle from first burn to location of first perfect formation geometry
Δv	= velocity changed used as a measure of fuel used
Q_R	= Robert-Roux tetrahedron quality factor (1=regular tetrahedron)
Q_G	= Glassmeier quality factor
$\int Q dt$	= integrated quality factor
T_{obs}	= observation time
S_i	= formation satellite ($i=1, 2, 3, 4$)
\mathbf{L}	= tetrahedron vertices vector ($L_1, L_2, L_3,$ and L_4)
P_i	= position of impulsive thruster firing ($i=1, 2$)
n	= number of design variables, or number of orbits
D	= amount of delay after firing thrusters before data can be collected
w	= weights applied to the terms of the cost function
J	= value of the cost function

I. Introduction

MISSION designs for satellite formations in orbit are typically categorized as either *natural* or *actively controlled*. Natural formations capitalize on the motion of spacecraft under central body gravitational forces to maintain certain geometries for at least a segment of a circular or elliptical orbit. The satellites in these formations do not use propellants to control their positions, except for a very occasional burn to correct orbit degradation.

* Graduate Research Assistant, Aerospace Engineering Department, Student Member, email: ahoskins@wam.umd.edu.

† Assistant Professor, Aerospace Engineering Department, Senior Member, email: atkins@glue.umd.edu.

Actively controlled formations are those in which individual satellites are expected to apply thruster forces to maintain a prescribed geometry through active three or six degree-of-freedom (DOF) control. The primary design goal for actively controlled formations is to avoid costly propellant usage while meeting formation geometric constraints, a challenging task for Earth-orbiting formations.

An early version of formation flight, Gemini 6 and 7 occupied approximately the same orbit to achieve low-fuel rendezvous. EO-1 and LandSat-7 successfully demonstrated the concept of formation flight with leader and follower where the follower automatically computes burns to maintain the designated separation.¹ A variety of natural orbit formation solutions have been proposed, with corrective burns applied infrequently to realign the satellite group.²⁻⁵ The concept of a virtual structure,⁶ virtual satellite,⁷ or virtual rigid body (VRB)^{8,9} has been developed to facilitate actively-controlled formation design and management, particularly when high-precision geometries must be maintained. With such a representation, each spacecraft acts as a “node” in an overall formation “structure” held together by natural and active control forces rather than by rigid physical components. In our previous work with the VRB concept,⁹ missions were designed such that the formation actively maintained perfect geometry over a particular region of each orbit, designated by width $\Delta\nu$ and center position ν_c as shown in Figure 1.

While VRB designs enable perfect geometry over an extended portion of each orbit, the use of continuous active thrust remains controversial. Current operational protocols require substantial mission support personnel whenever spacecraft burns are executed. Additionally, thruster emissions may compromise data from sensitive science instruments. The objective of this research is to investigate a novel satellite formation mission design strategy that maximizes geometric quality through the use of infrequent impulsive thrust commands. With this multi-impulse design strategy, impulses are applied to initiate orbits that maximize future formation quality and minimize fuel use over all required impulses. The distinction of this work is that we actively optimize impulse application as part of the mission planning process, as opposed to designing the best possible natural formation and then applying impulses when necessary to correct for perturbations. Our hypothesis is that the opportune application of low-magnitude impulses can improve overall science data quality (formation geometry) with acceptable fuel use.

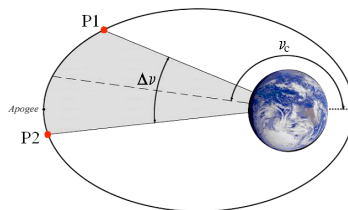


Figure 1: VRB / Dual-Impulse Formation Design Strategies.

The multi-impulse design strategy is applied to the Magnetospheric Multi-Scale (MMS) mission, a tetrahedral four-satellite formation in a highly elliptical orbit.¹⁰⁻¹³ Following a description of the MMS multi-impulse mission design problem, we present two algorithms that were tasked with MMS optimization: a hierarchical method used in our previous work and a particle swarm optimization algorithm. The results presented in this paper use optimization to solve two problems. The first is a dual impulse solution presented as a compromise between natural orbit and VRB solutions. The problem is then extended to include reconfiguration of the formation between impulsive thruster firings. Due to computational complexity issues, we utilize a purely Keplerian model of dynamics for our optimization processes. A simulator with perturbations is incorporated into the final stage of our mission design process. This paper derives perturbed solutions from the optimal Keplerian design vectors and compares their fuel use and geometric quality with the original Keplerian results.

II. MMS Formation Optimization Problem Definition

To define the multi-impulse optimization design vector, a series of reference frames analogous to those defining a VRB are utilized. First, an inertial frame is placed at the center of the Earth. The x-axis points to the vernal equinox, and the z-axis points to the North Pole. A target (**T**) frame is assigned a natural orbit defined by orbital elements (a , e , i , $\tilde{\omega}_{true}$, and ν .) For this paper the **T**-frame is assigned an equatorial orbit. The right ascension of the ascending node is therefore not defined, and that angle is combined with the argument of perigee to create the true longitude of perigee ($\tilde{\omega}_{true}$). The **T**-frame has the same attitude as the initial inertial frame. The final reference frame, the vehicle (**V**) frame, has its center offset from **T** by values V_x , V_y , and V_z and is aligned in attitude with **T**.

Several MMS design problems were investigated. All problems presume a regular tetrahedron geometry with a satellite occupying each vertex node. The distance between each of the satellites is 10 km, one of the sizes specified

for MMS. As shown in Figure 2, the formation is oriented so that the location of vertex one (L_1) is on the y-axis of the V-frame. L_2 and L_3 are equidistant from the center of the V-frame parallel to the x-axis, and L_4 is located on the V-frame z-axis.

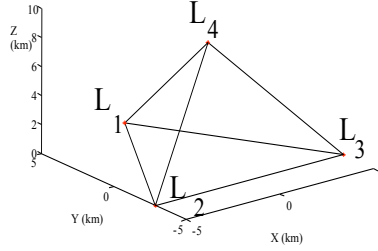


Figure 2. Satellite Offsets from V-frame

The following assumptions were made for all formation optimization processes:

- 1) Satellite motion is only influenced by Keplerian forces. Although perturbing forces will vary satellite motions, general trends will remain unchanged and the inclusion of perturbing forces makes optimization intractable. Differences between the Keplerian solution and the equivalent solution simulated under a more complete force set are presented to quantify the effect of this assumption for our MMS designs.
- 2) Instantaneous Δv is possible. This assumption allows us to use Lambert's solution to calculate the Δv needed to travel between P_1 and P_2 .
- 3) Thrust is possible in any direction at any time without the need to reorient the satellite.
- 4) If the calculated Robert-Roux quality factor (Q_R)¹⁴ value is above 0.7, then data can be collected. Otherwise, no data can be collected. The Robert-Roux quality factor is the sole measure of tetrahedron quality for this work; functioning similarly to comparable measures such as the Glassmeier parameter (Q_G)¹⁴.

Orbital elements for the reference T-frame were defined in accordance with MMS mission specification¹² and were presumed the same for each optimization result presented in this paper. The semi-major axis (a) is 61,230.144 km, the eccentricity (e) is 0.875, and, as was mentioned above, the inclination (i) is set to 0°. All design problems required optimization over parameters $\tilde{\omega}_{true}$, V_x , V_y , and V_z . In addition, optimal values for Δv and v_c (Figure 1) were identified, defining the orbit reference locations where burns P_1 and P_2 are applied.

Symmetries were identified to minimize design variable search spaces Δv and v_c that each ranged from 0°-180°. $\tilde{\omega}_{true}$ also originally ranged from 0-180° but was readjusted to $\pm 30^\circ$ range. With the constant tetrahedron orientation presumed for this work, a $\tilde{\omega}_{true}$ rotation of 60° changes the apparent locations of the in-plane satellites (L_1 , L_2 , and L_3).

All design problems presume all four satellites start in the Figure 2 configuration at orbital station P_1 with the same velocity as the T-frame. Without reconfiguration, the satellites are constrained to be in the same configuration when the T-frame reaches P_2 with velocities again matching the T-frame velocity. To achieve this goal, Lambert's method is used to calculate the required impulses for each satellite. The satellites are not controlled during the transit from P_1 to P_2 . The same methodology is used to calculate the Δv 's for the satellites to perfectly reassemble at P_1 in their original configuration. Optimization of formation attitude at P_1 and P_2 was not performed in this work.

With reconfiguration, discrete location vector $\mathbf{L} \{L_1, L_2, L_3, L_4\}$ (Figure 2) is added to the optimization design vector to match satellites with orbital stations after the P_1 - P_2 transition and again after the P_2 - P_1 transition that completes the single orbit over which the formation is optimized.[‡] Without reconfiguration, effectively $\mathbf{L}_0 = \mathbf{L}_{P1} = \mathbf{L}_{P2} = \{S_1, S_2, S_3, S_4\}$. Reconfiguration allows for 24 possible combinations of satellite positionings as they transit between perfectly assembled stations.

Equation (1) shows the cost function developed for previous work in VRB optimization⁹ that is also adopted for this work:

$$J = w_1 \left(\sum_{Q_{R,i} \approx Q_{R,\min}} Q_{R,i} \cdot \Delta t \right) + w_2 \left(\sum_{Q_{G,i} \approx Q_{G,\min}} Q_{G,i} \cdot \Delta t \right) + w_3 \left(\frac{\Delta v}{T_{obs}} \right) \quad (1)$$

[‡] At the end of the first orbit, the satellites are constrained to form a tetrahedron with the T-frame velocity. Since all satellites are presumed identical, the problem effectively resets after one orbit even though S_1 may not have returned to L_1 , etc.

where w_1, w_2, w_3 are weighting factors, Q_R is the Robert-Roux quality factor, Q_G is the Glassmeier quality factor, $Q_{R,min}, Q_{G,min}$ are minimum acceptable values of Q_R and Q_G , $(Q_{R,i}, Q_{G,i})$ are Q_R and Q_G at station i in the orbit, Δt is the orbit propagation time step, Δv is the total Δv applied around the orbit, and T_{obs} is the time of observation per orbit. As will be discussed below, three primary weight combinations are used for this work. One set optimized over quality factor Q_R only with weights $(w_1=-1, w_2=0, w_3=0)$, while a second set minimized fuel use with weight vector $(w_1=0, w_2=0, w_3=1)$. The final set has $w_1=-1, w_2=0$, and $w_3=1.3*10^{12}$, a compromise scaled to approximately balance fuel and quality factor influences. Note that w_1 is negative because quality factor is maximized.

III. Optimization Methods

A host of local minima are present for the MMS mission design problem studied in this work. Although no algorithm is perfect, we attempt to explore a diverse solution space via two very different optimization strategies: a hierarchical algorithm developed in our previous work and a particle swarm optimization approach with genetic algorithm heritage. A comparison of results will enable the adoption of the best solution over these two optimization approaches. Both methods are desirable for this problem because they do not require knowledge of cost function derivatives. Both are also attractive compared to classical methods because they examine a large portion of the search-space, which reduces the likelihood of becoming trapped at a local minimum.

Hierarchical Optimization

The hierarchical optimization algorithm performs a multi-stage search to identify the best solution. Given a coarse search grid, an initial exhaustive search is performed to identify the regions in which local minima might reside. Next, the lowest-cost coarse search design vectors are locally optimized, and the coarse grid is refined until the region in which the local minimum resides is identified. The refinement process iterates until the algorithm is convinced it has found the globally optimal solution. As a check for optimality, the initial coarse grid is shifted and the hierarchical algorithm is again executed, with the coarse grid itself refined until the shifted-grid solution matches its unshifted counterpart. A more detailed description of this method can be found in Ref. 9.

As discussed in previous work, the hierarchical method only converges on the global minimum if the search grid is properly selected or may be sufficiently refined. It has been observed that for satellite formation design problems with numerous local minima, changing the weights of the cost function significantly changes the number and locations of local minima, which increases the difficulty in identifying the globally optimal solution. Adding additional search parameters also increases computational complexity substantially. Thus, we have adopted a second method, providing a comparison of algorithm performance and solutions found by each.

Particle Swarm Optimization (PSO)

Particle swarm optimization (PSO) is a stochastic optimization method that can rapidly explore large regions of the design vector solution space. It has been proven to be a reliable method to identify solutions for a variety of different applications.¹⁵⁻¹⁷ Each design variable x_i has range $[x_i^{min}, x_i^{max}]$, and no constraints are imposed. The amount a variable can change between iterations lies within $[v_i^{min}, v_i^{max}]$. The optimization steps are outlined below and illustrated in Figure 3.

1. *Randomly generate the initial population.* A predefined number of candidate solutions (particles) and the initial velocity of each particle are randomly generated. The cost of each particle is calculated and a vector containing all n design variable values and the cost for that design vector is created.

2. *Compare cost of particles.* The algorithm has a memory of the best location each individual particle has ever occupied. The vector $\mathbf{p}_{best,i}$ (where i represents particle number) contains the cost associated with that location along with the design variables that represent the location. All $\mathbf{p}_{best,i}$ vectors are initialized to be the starting location of each particle. The algorithm also has a memory of the best location any particle has ever occupied. To initialize this vector, the $\mathbf{p}_{best,i}$ vectors are compared and the vector associated with the minimum-cost particle is copied to a vector referred to as \mathbf{g}_{best} .

3. *Iteration process.* Equation (2) is used to update the velocity of every particle in every dimension.

$$v_{j+1} = \omega v_j + \frac{c_1 r_1 (p_{best} - x_j) + c_2 r_2 (g_{best} - x_j)}{\Delta t} \quad (2)$$

where v_{j+1} is the new velocity, ω is the inertial weight, v_j is the current velocity, c_1 and c_2 are weighting factors, r_1 and r_2 are random factors, p_{best} is the value from the $\mathbf{p}_{best,i}$ vector associated with the dimension being updated, x_j is the current position of particle i in dimension j that is being updated, g_{best} is the value from the \mathbf{g}_{best} vector associated with dimension j , and Δt is the time step.

The values of c_1 and c_2 are referred to as the cognitive and social parameters respectfully and can be used to cause the particle to have a tendency to fly past the $\mathbf{p}_{best,i}$ and \mathbf{g}_{best} locations. They can also be used to show preference to either the p_{best} or g_{best} term. For this research, all of the c_1 and c_2 values were set to 2. This selection allowed the particle to potentially overshoot the best location, a choice that created a varied search pattern. The range of r_1 and r_2 is $[0, 1]$. This adds another random element into the problem. Δt is always set to 1. ω is a critical parameter to select for the tradeoff between execution time and result quality: a large value will create a coarse search while a smaller value will result in a more refined search.

After the velocity of a particle is updated in a dimension, the position of that particle, in that dimension, is also updated via a first-order integration step. After the location for each particle dimension has been computed, particle cost is updated accordingly. The new cost is compared with the previous $\mathbf{p}_{best,i}$ cost, and if the new cost compares favorably $\mathbf{p}_{best,i}$ is updated. After all particles are updated for the given iteration, the costs of all of $\mathbf{p}_{best,i}$ vectors are compared to the \mathbf{g}_{best} cost. If a better solution has been found, then \mathbf{g}_{best} is updated.

4. *Check stopping criteria.* The PSO process will terminate if either the algorithm has converged to a solution or if the maximum number of iterations is exceeded. If neither condition has been met, step three is repeated.

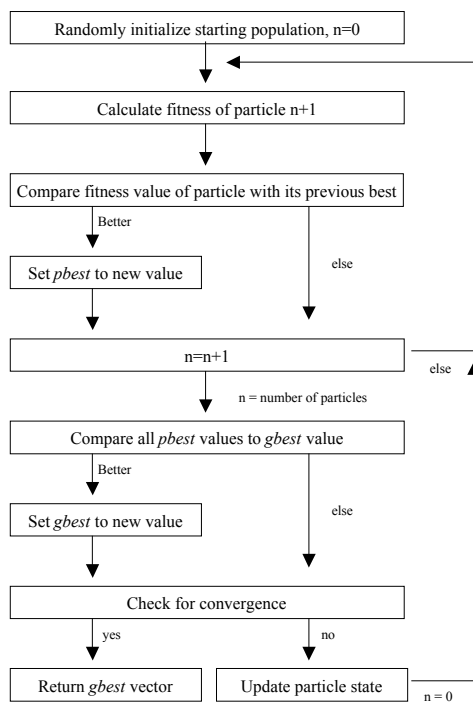


Figure 3. PSO Method

IV. Dual Impulse Designs

An initial dual-impulse design strategy derived from VRB results⁹ constrained the formation to form a perfect tetrahedron at the two burn locations. The pair of transitions between the two perfect locations was determined by applying Lambert's solution for each transition. The hierarchical optimization algorithm was utilized to find the minimum cost solution. In this work, a series of optimizations were performed to evaluate the effects of cost function weight variations on the solution. Also, to account for disruption in the local magnetic field when thrust is applied, a delay (D) was introduced and assigned one of two values: $D=0$ (no delay) and $D=3600$ (observation delay of one hour after impulsive thrust is applied). We hypothesize that an hour will be an upper bound on delay time because thruster emissions will disperse and because the spacecraft itself will move away from the disturbed area.

Figure 4 shows the evolution of quality factor for this series of one-orbit dual-impulse tests, with the T-frame as the universal time clock in all plots. Table 1 summarizes the numerical results. All distances are in kilometers and velocities are in km/sec. For the Table 1 results, bounds of $\pm 10,000$ km were placed on V_x , V_y , and V_z to enable discovery of optimal solutions further from the T-frame reference orbit. For all cost function weights, as expected, a non-zero D increases cost (i.e., makes cost less negative) by excluding observation regions near the thrust application sites where geometry is most perfect. However, the remaining valid observation time per orbit (>80% for

most cases) is still significantly higher than the 34.4% observation time per orbit with the optimized natural orbit solution identified in previous work.⁹

Several conclusions can be drawn from the Table 1 results. First, the optimizer had significant freedom to alter satellite orbits with large V -frame offsets. With only Qdt cost, a solution was identified that allowed the formation to use large offsets to better align satellites across the drift periods. These Qdt solutions (Tests 1 & 2) are not attractive, however, because of the significant Δv required. Perhaps the most surprising result was achieved in Test 3 ($\Delta v/T_{obs}$ cost, no delay), illustrated in Figure 5. Because quality is not included in the cost function, the optimizer chose a solution that met the constraint of “perfect geometry at impulse sites”, but the formation immediately diverged from a tetrahedron due to the out-of-plane Satellite 4 orbit. This solution is not acceptable from a quality factor perspective, but the optimizer did its job, requiring a Δv many orders of magnitude less than other solutions.

Test 4 ($\Delta v/T_{obs}$ cost, $D = 1$ hour) could not adopt the low-fuel result from Test 3 because no region with $Q_R > 0.7$ was present outside the area contaminated by thruster use (i.e., $T_{obs} = 0$). An alternate solution was identified that required significantly more fuel but had non-zero observation time. This solution is similar to results that include Qdt cost but with somewhat lower integrated quality factor and Δv . The most promising one-orbit dual-impulse solution, Tests 5 and 6 in Table 1, utilizes the cost function with both fuel use and quality factor terms. With no delay, observation can occur over 87% of the orbit with reasonable fuel use, and with delay, a comparable solution is found but observation time (82%) is reduced by the delay period following thruster use.

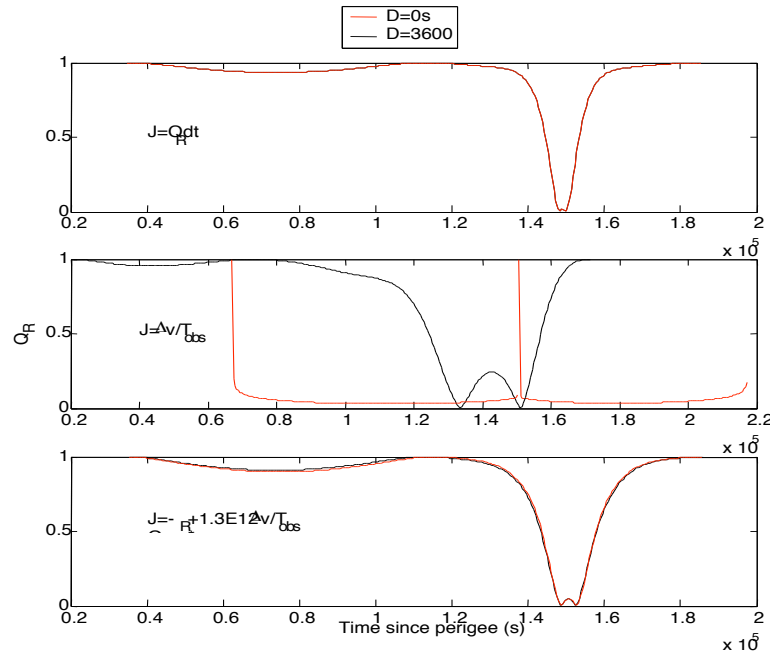


Figure 4: Single-orbit Dual Impulse Quality Factor Evolution

Table 1: Single-orbit Dual Impulse Solution Summary

Input:			Solution:							Statistics:			
Test #	Cost	Delay	Δv (rad)	v_c (rad)	$\tilde{\omega}_{true}$ (rad)	V_x (km)	V_y (km)	V_z (km)	Δv (km/s) / orbit summed over all sats	Qdt (total)	T_{obs} %	Cost (J)	
1	Qdt	0	0.5132	3.128	8.69E-04	-9999	9896	-9788	4.23E+00	134737.9	92.52%	-1.35E+05	
2	Qdt	1hr	0.5132	3.128	8.69E-04	-9999	9896	-9788	4.23E+00	126744.5	87.21%	-1.27E+05	
3	$\Delta v/T_{obs}$	0	3.1409	1.522	1.10E+00	-3.71	-14.15	-3.07	2.46E-10	1999.999	0.66%	2.46E-13	
4	$\Delta v/T_{obs}$	1hr	0.4205	2.917	2.22E-01	0.08	-4.12	115.9	7.31E-04	99147.72	69.30%	7.00E-09	
5	Both	0	0.5045	3.130	2.30E-02	-0.36	50.55	-208.7	9.6E-04	124945.1	87.21%	-1.15E+05	
6	Both	1hr	0.5258	3.137	6.38E-03	0.61	-1.68	332.3	9.83E-04	117051.9	82.24%	-1.07E+05	

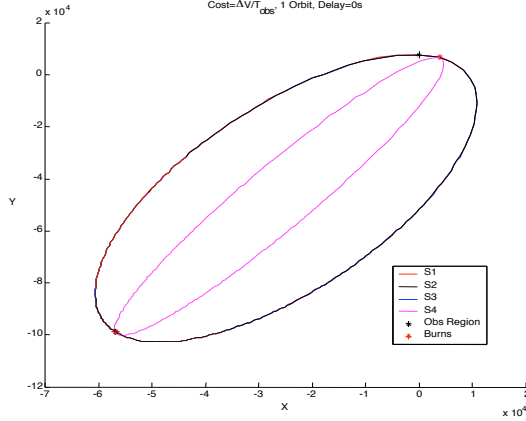


Figure 5: One-orbit Solution with $\Delta v/T_{obs}$ cost only, No Delay, $|V_{i,max}|=10000\text{km}$

Next, we studied application of a multi-revolution Lambert’s solution impulse pair across multiple orbits such that, on average, one or fewer impulses are required per orbit. The geometry was constrained such that the formation is perfect at each thrust application site, and that after n orbits ($n=2,3$, or 4 in our tests), the formation returns to its initial state so that the trajectory pattern can be repeated. A summary of results is shown in Table A1. Use of different cost function weights produced similar numerical results as the one-orbit case: high fuel use with only quality factor (Qdt) as cost, lower fuel use and quality factor when only considering $\Delta v/T_{obs}$, and a compromise solution generated when considering both quality and fuel. Unlike the one-orbit cases, however, all the multi-orbit solutions favored large V offsets. Such offsets are likely undesirable given the science data requirements upon which the original T -frame a and e values were based. Upon close inspection of the orbits for multi-orbit cases, the large V -frame offsets are significantly changing the orbit properties relative to the reference T - frame. Maintaining a near-regular tetrahedron thus appears to require more than one impulse per orbit and multi-orbit solutions are not pursued further in this paper.

Table 2: Solutions with Perfect Geometry Away from Impulse Application Stations

Test	Delay	Δv (rad)	v_c (rad)	vp (rad)	$\tilde{\omega}_{true}$ (rad)	V_x (km)	V_y (km)	V_z (km)	Δv (km/s)	T_{obs} %	Cost
25	0	0.40	3.00	$\Delta v/2$	2.52	-13.50	50.00	-3000.00	8.93E-04	64%	-8.05E+04
26	1 hr	0.35	3.14	$\Delta v/2$	2.52	-10.91	-22.50	-522.90	1.15E-03	71%	-8.62E+04
27	0	0.89	2.94	0.67	2.52	7.29	9.17	212.71	1.23E-03	69%	-8.31E+04
28	1 hr	0.90	2.93	0.69	2.52	8.73	11.68	98.62	1.21E-03	66%	-7.87E+04

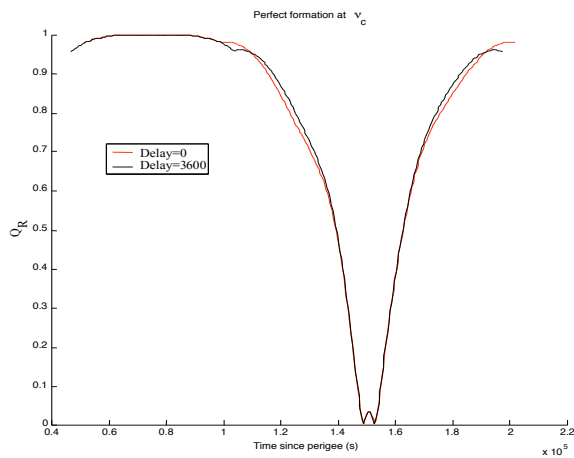


Figure 6: Formation with Perfect Geometry at v_c

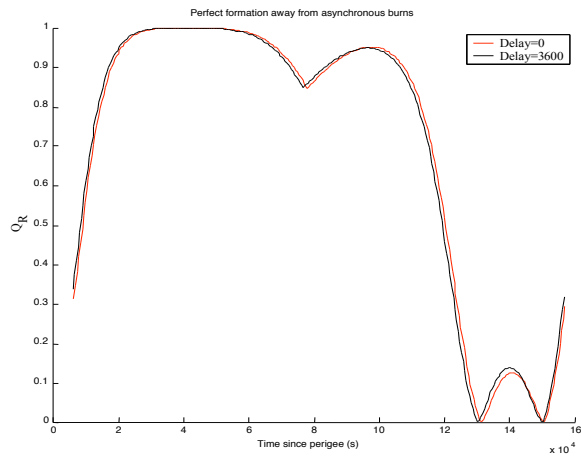


Figure 7: Asynchronous Results

Single-orbit designs presented thus far require the formation to achieve perfect geometry at the impulse application sites. However, because of possible science instrument contamination from thruster emissions, no data can be taken while the formation is a perfect tetrahedron. Therefore, designs were investigated in which the formation was allowed to perfectly assemble at stations other than the impulse application sites.

Test cases 25 through 28 (shown in Table 2) describe the results of this analysis. Figure 6 illustrates quality factor over an orbit for Tests 25 and 26 in which formation geometry was constrained to be perfect at v_c rather than the impulse application sites. Although the quality factor is near perfect around apogee ($\sim v_c$), there is less total observation time compared to the Test 6 design because Q_R degrades below 0.7 more quickly given no constraint to have perfect geometry at impulse application sites. Note, however, that with a higher threshold ($Q_{R,min}$ closer to 1.0), Test 26 may out-perform the Test 6 design given the extended-duration near-perfect geometry around apogee. For the next set of tests, a parameter v_p was included in the search space to identify the best single location for perfect geometry over the orbit. Angle v_p is defined as zero at the initial impulse application site, P_1 . The results are listed in Table 2, with quality factor for delay and no-delay cases plotted in Figure 7. Much like the previous case (Figure 6), the new “asynchronous” solutions (Figure 7) maintain near-perfect geometry for longer periods of time than their Test 6 counterpart. However, in both asynchronous cases, quality factor drops below 0.7 well before perigee, again indicating that the original (Test 6) solution is the best solution given $Q_{R,min}=0.7$.

V. Hierarchical Optimization versus PSO

The above results were obtained using the hierarchical optimization method. The same tests were repeated using the PSO algorithm. Table 3 shows a comparison of the hierarchical versus PSO results. As can be seen in the table, the two methods converge to answers with approximately the same cost with each method outperforming the other in some cases. The PSO algorithm had to be run several times because there is no guarantee that any single answer will be the global minimum. The hierarchical method is dependent on the initial coarse search grid. Because the number of local minima is not known a priori, this method may also require multiple executions to guarantee that it has found the global minimum. As a result, the time needed for each algorithm to find the global minimum is not known exactly, but the two methods executed with comparable speed for the MMS design scenarios described above. However, as the search space expands, PSO does not have a significant increase in the amount of time needed to reach convergence while the hierarchical method does. A combined approach that uses both methods will help to ensure that the identified solution is at least close to the global minimum solution.

VI. Reconfiguration Problem Results

To improve the cost, we investigated swapping satellite nodes during transit between the orbital stations; this increased the search space beyond the reasonable size the hierarchical search could handle. Others have studied analogous reconfiguration strategies in the past¹⁸. The tetrahedron is a symmetric structure, and all formation satellites are identical. However, as a simplification, our previous results assumed satellites would return to their original tetrahedron vertices, and that the tetrahedron would always assemble at the same attitude relative to an Earth-centric inertial coordinate frame. The four satellites, S_1 , S_2 , S_3 , and S_4 , initially occupy tetrahedron vertices L_1 , L_2 , L_3 , and L_4 at P_1 (see Figure 2). Results prior to this section have had the satellites occupy the same tetrahedron vertices at P_2 . However, there is no reason to assume that this configuration is optimal. Allowing satellites to reconfigure at any combination of vertices significantly increases the total search-space size. There are $4!$ possible reconfigurations from P_1 to P_2 . When possible reconfigurations from P_2 back to P_1 are also considered, then the two reconfiguration problems together have $4!^2=576$ possible solutions, multiplying the overall search-space size by this same factor. As a result, optimization time can easily increase beyond reasonable limits of single-processor execution and only the PSO algorithm was able to optimize this dual-impulse design problem within a reasonable time. Reconfiguration was viewed as a simplified way to approach the concept of changing the formation attitude. Results of optimizing MMS formation attitude at impulse application sites will be presented at the NASA Goddard Flight Mechanics Symposium in October¹⁹.

Forty independent PSO runs were executed with maximum \mathbf{V} -frame offsets set to ± 10 km and $w_1=-1$, $w_2=0$, and $w_3=1.3*10^{12}$. All returned solutions that were not discarded contained one of three of the possible 576 reconfiguration sets. The best returned solutions were defined as any returned solution that had a cost lower than $-1.14*10^5$, identified through an analysis of PSO solution clustering as a reasonable cutoff. These returned solutions accounted for ten of the forty returned solutions; the remaining PSO solutions were discarded. All three sets were chosen approximately the same number of times. Further inspection of the sets revealed that they could all be explained by the same process and produced identical quality factor results. There are three satellites in the same plane and one satellite out-of-plane. For the transition from the initial location to the end of Δv (P_1 to P_2), the

satellites maintain the same tetrahedron vertices. For the transition from P_2 back to P_1 , the out-of-plane satellite swaps positions with one of the other three satellites, while the other two satellite vertices are unchanged.

Figure 8 compares the quality factor between the reconfiguration solution and the original solution. Both solutions had $w_1=-1$, $w_2=0$, and $w_3=1.3*10^{12}$. The out-of-plane position swap helps maintain tetrahedron geometry after P_2 . The most significant reason the quality factor decreases near perigee is the motion of the out-of-plane satellite. The local maximum near perigee seen in the no reconfiguration solution near 150,000 seconds is caused by the out-of-plane satellite passing through the plane of the other three satellites, reaching a maximum distance from that plane, and then passing back to its usual side of the plane. By having the two satellites switch to/from the out-of-plane station, the four orbits are more similar, so the formation has a greater Qdt value. However, the initial movement of the swapped satellites causes the formation to initially degrade quality factor slightly more than in the original solution.

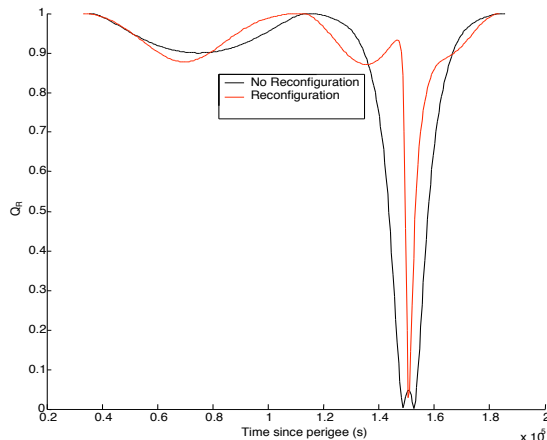


Figure 8: Quality Factor for Reconfiguration versus No Reconfiguration with Quality Factor Preference.

Table 3: Comparison of Hierarchical Optimization and PSO Results

	<i>Test 1</i>	<i>Test 2</i>	<i>Test 3</i>	<i>Test 4</i>	<i>Test 5</i>	<i>Test 6</i>	<i>Test 7</i>	<i>Test 8</i>
Hierarchical Cost	-1.35E+05	-1.27E+05	2.46E-13	7.00E-09	-1.15E+05	-1.07E+05	-2.61E+05	-2.53E+05
PSO Cost	-1.36E+05	-1.29E+05	2.59E-11	4.60E-09	-1.18E+05	-1.07E+05	-2.11E+05	-2.03E+05
	<i>Test 9</i>	<i>Test 10</i>	<i>Test 11</i>	<i>Test 12</i>	<i>Test 13</i>	<i>Test 14</i>	<i>Test 15</i>	<i>Test 16</i>
Hierarchical Cost	6.54E-09	5.20E-09	-1.67E+05	-1.59E+05	-3.54E+05	-3.48E+05	1.57E-08	1.69E-08
PSO Cost	4.00E-09	3.98E-09	-1.39E+05	-1.31E+05	-2.52E+05	-2.44E+05	1.03E-08	1.08E-08
	<i>Test 17</i>	<i>Test 18</i>	<i>Test 19</i>	<i>Test 20</i>	<i>Test 21</i>	<i>Test 22</i>	<i>Test 23</i>	<i>Test 24</i>
Hierarchical Cost	-5.47E+04	-2.43E+04	-3.61E+05	-3.53E+05	1.18E-08	1.62E-08	-4.77E+04	-3.42E+04
PSO Cost	-5.51E+04	-4.62E+04	-2.33E+05	-2.25E+05	1.02E-08	1.23E-08	-4.39E+04	-3.57E+04

With the weights of the cost functions set at $w_1=-1$, $w_2=0$, and $w_3=1.3*10^{12}$, Q_R had more influence on the candidate solution than the $\Delta v/T_{obs}$ term. An investigation of the impact of a more equal weighting of the terms in the cost function seemed warranted. For the remainder of the results presented in this paper, cost function weights are set to $w_1=-1$, $w_2=0$, and $w_3=1.3*10^{13}$. At first $\tilde{\omega}_{true}$ had was searched from 0 to 180°, but when the search space was adjusted to be $\pm 30^\circ$ optimal values that were more consistent than previous results had indicated were achieved. For most optimization processes, the optimal value of Δv ranged between 0.4 and 0.9 radians depending on the weights of the cost function. The value of v_c was shown to be approximately π radians (apogee). These values seem logical because burns are usually applied near apogee and these values place the burns near apogee. Once $\tilde{\omega}_{true}$ was constrained properly, a constant value was identified in optimal solutions. For the reconfiguration problem with the above-mentioned parameters, a value of approximately 0 radians was returned for $\tilde{\omega}_{true}$.

The V-frame offsets had also exhibited inconsistency in previous results. However, data runs with the weights mentioned above applied to the cost function and a properly constrained $\tilde{\omega}_{true}$ search space indicated that the value of V_x should be approximately 0 km. Because $\tilde{\omega}_{true}$ was found to be 0.0 radians, the semi-major axis of the T-frame orbit lies on the x-axis. The period of an orbit is determined by the semi-major axis of the orbit. To reduce the

needed amount of fuel, the satellite orbits from P_1 to P_2 and from P_2 to P_1 will be similar to the **T**-frame orbit because the time between the points is constrained to be the time an object on the **T**-frame orbit would take to travel between the points. In order for the satellites to have similar orbits to the **T**-frame orbit, the semi-major axes of all five orbits must be similar. The V_x offset is along the semi-major axis, so it is therefore optimal at ~ 0 km.

When the value of $\tilde{\omega}_{true}$ was constrained properly, the optimized reconfiguration solutions also converge to a single solution for each successfully PSO iteration. This optimal reconfiguration vector again exhibits no change in the configuration from P_1 to P_2 and then has S_2 and S_3 change positions from P_2 back to P_1 while S_1 and S_4 remain in the same tetrahedron vertices.

The reason this reconfiguration set returns the best result is due to fuel usage. A difference between the semi-major axis of a satellite's orbit and the **T**-frame orbit causes the period of the satellite's orbit to be different from the **T**-frame. The amount of time an object would take to move between the two locations on the **T**-frame orbit is the time the satellites have to move between the two locations. For reasons analogous to the explanation for $V_x = 0$ km, all of the satellites would not have an offset from V_x . The satellites at L_1 and L_4 do not have an offset from V_x and require very little fuel for either the reconfiguration or the original problem. The satellites at L_2 and L_3 do have a non-zero offset, so their semi-major axes are not quite identical to the **T**-frame semi-major axis. As a result, fuel is used to correct for this difference in orbital periods. By having the satellite with the shorter period take the position of the satellite with the longer period, the velocity on arrival is closer to the velocity of the **T**-frame, so less fuel is needed at the burn location.

However, the crossing of the satellites does decrease quality factor. When going from P_2 to P_1 , the quality factor drops due to the movement of the out-of-plane satellite, so the crossing of S_2 and S_3 does not change the quality factor in a significant way. If the satellites were to cross while traveling between P_1 and P_2 , then the quality factor would change and the design would not be viewed as a more optimal solution.

V_y and V_z do not have a significant impact on the solution. There were 329 returned solutions at the apparent global minimum with the properly constrained $\tilde{\omega}_{true}$. Six of the eight variables had standard deviations less than 2%

of the searched region. The other two, V_y and V_z , are random. Table 4 summarizes the results of the 329 "good" PSO candidate solutions. V_y and V_z were constrained to be between ± 10 km. No equation was found to properly describe the relationship between V_y and V_z . Figure 9 is the plot of the values, which indicates the values of V_y and V_z do not significantly influence overall design cost for the dual-impulse MMS design with reconfiguration.

Table 4: PSO Candidate Solutions Near Global Minimum

	<i>Max</i>	<i>Min</i>	<i>Mean</i>	<i>Std</i>	<i>Std %</i>
<i>Iterations</i>	5486	1759	3176.723	783.47	-
<i>Global Best (eqn 1)</i>	-86940.68	-87195.73	-87153.99	34.24	-
Δv (rad)	0.9352	0.8898	0.9111	0.0098	0.64
v_c (rad)	3.1416	3.1120	3.1324	0.0065	0.42
$\tilde{\omega}_{true}$ (rad)	0.0296	-0.0004	0.0091	0.0065	1.24
V_x (km)	0.0050	-0.0024	0.0007	0.0017	0.02
V_y (km)	10.00	-10.00	0.32	6.80	68.0
V_z (km)	10.00	-10.00	0.69	7.20	72.0

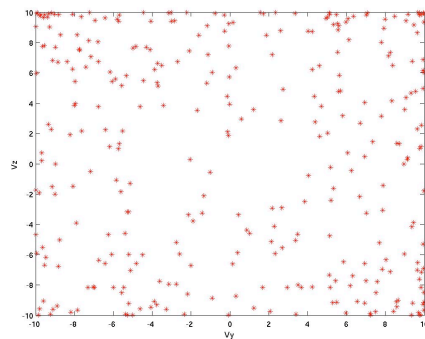


Figure 9: V_z vs. V_y for the Refined Solution

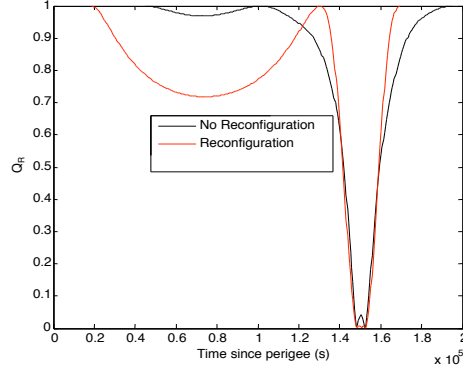


Figure 10: Quality Factor for Reconfiguration versus No Reconfiguration with Minimum Fuel Preference

Figure 10 shows a plot of the quality factor versus time for the solution with the weights of the cost function set to $w_1=-1$, $w_2=0$, and $w_3=1.3 \times 10^{13}$. When Figure 8 is compared to Figure 10, the influence of the weighting factors on the optimal solution becomes apparent. In Figure 10, Δv has a value that allows the quality factor between P_1 and P_2 to drop to approximately the minimum quality factor value of 0.7.

The no reconfiguration solution of Test 6, ($w_1=-1$, $w_2=0$, $w_3=1.3 \times 10^{12}$, $D=1$ hour, no reconfiguration, and perfect geometry at P_1 and P_2) does not require as much fuel use as the reconfiguration problem, but also provides less observation time. The reweighted solution above ($w_3=1.3 \times 10^{13}$) uses less fuel, but has a reduced average quality and less observation time. These results are summarized in Table 5.

Table 5: MMS Design Comparison

	<i>No Reconfig</i>	<i>Reconfig. Higher Qdt</i>	<i>Reconfig. Higher Dv/Tobs</i>	<i>Simulation</i>	<i>Iterated Simulation</i>	<i>SDP4</i>
Cost	-1.07E+05	-1.14E+05	-9.38E+04	-	-	-
Total Δv (km/s)	9.83E-04	1.63E-03	6.20E-05	1.94E-02	1.54E-02	2.46E-03
Tobs %	82.2%	92.2%	80.9%	82.1%	82.2%	81.9%
Average Q	0.9440	0.9281	0.8233	0.9400	0.9395	0.9448
Reconfiguration	No	Yes	Yes	No	No	No
Optimized	Yes	Yes	Yes	No Reconfig Soln	No Reconfig Soln	No Reconfig Soln

VII. Simulation Results

The assumption that the only forces acting on the satellites are Keplerian allowed us to efficiently identify candidate MMS designs. Both the PSO and hierarchical methods investigate millions of solutions for each design problem, and without the Keplerian assumption computation time would be prohibitive. However, the perturbing forces are not insignificant and must be taken into consideration for the final design. A simulator²⁰ that applies lunar perturbations, atmospheric drag, and the J_2 - J_5 forces was applied to the “baseline” MMS design obtained in Test 6 (Table 1). This baseline solution was selected because it was observed to provide balance between quality and fuel use, as well as conservatively modeling data collection interruption near impulse application sites. Reconfiguration and v_p were not included in this comparison between Keplerian and simulated solutions so that a baseline for perturbing force impact could be straightforwardly established.

The formation was initially placed at orbital station P_1 in its configuration from Figure 2 and the velocity of each satellite was set to the velocity that had been determined using Lambert’s method to set up the next drift orbit segment. At orbital station P_2 , the velocities of the satellites were adjusted so that they were the values determined using Lambert’s method. As shown in Table 6, a position error (Δx , Δy , Δz) between the estimated two-body solution and the simulator results exists. The required Δv is significantly higher than the previously calculated values. The first three Table 6 columns show differences in positions, the second set of three columns contain the Δv ’s calculated using Lambert’s method, and the final columns list Δv ’s the simulator applied to achieve the desired velocities (given the Keplerian design) at orbital stations P_1 and P_2 .[§]

[§] Velocities varied significantly after each drift period, and it was observed that quality factor degraded to near-zero after the first burn at P_1 when velocities were not matched with those identified during the Keplerian optimization process.

Figure 11 provides a comparison between the quality factor plot of the original solution and the simulation results. As can be seen, even though there is a change in the position and the required Δv 's, the formation geometry does not change during the orbit relative to the initial estimated solution. The assumption had been made that the satellites would return to the initial positions once per orbit. However, the perturbations disallow that assumption. To investigate the impact of the change in position, the simulator was used to change the velocity each time the formation returned to P_1 and P_2 over the course of a month. These results indicate that the amount of Δv needed changes with each new orbit and that the position errors also change. For our simulation, total required Δv is 769 m/s for orbit 18, compared to 19 m/s for orbit 1. The general trend was a continual increase in fuel requirement with low-magnitude oscillatory behavior; a Δv peak occurred during orbit 16 where it was almost 6 km/s. The total position error at P_1 and P_2 for orbit 1 was 692 km as compared to 10,861 km for orbit 18. The trend in the total position error is the same as the fuel requirements with a peak position error of over 170,000 km for orbit 16.

The greater Δv , as compared to the planner solution, is needed, in part, because of the position error. The difference in the positions places the satellites on different orbits. The two sets of orbits (Keplerian and simulator) have different velocities. The velocities needed for the transfer orbits are more similar to the theoretical orbit than they are to the actual orbit. As a result, more fuel is needed to change to the transfer orbit. By correcting the position error, the velocity error should be less since the actual orbit will be in closer agreement with the theoretical orbit, and less Δv should be needed.

Table 6: First Orbit Perturbed Simulation Results

$P1$	Δx (km)	Δy (km)	Δz (km)	Lambert Δvx (km/s)	Lambert Δvy (km/s)	Lambert Δvz (km/s)	Simulation Δvx (km/s)	Simulation Δvy (km/s)	Simulation Δvz (km/s)
S1	-6.82	116.28	-3.88	0.00E+00	0.00E+00	0.00E+00	2.03E-03	2.05E-03	2.31E-04
S2	-6.86	116.29	-3.88	-1.86E-04	-1.63E-04	1.00E-06	2.21E-03	1.89E-03	2.30E-04
S3	-6.91	116.08	-3.88	1.85E-04	1.62E-04	-1.00E-06	1.85E-03	2.21E-03	2.32E-04
S4	-6.83	116.26	-3.92	-2.00E-06	-1.00E-06	0.00E+00	2.03E-03	2.05E-03	2.31E-04
$P2$									
S1	52.92	17.83	9.80	0.00E+00	0.00E+00	0.00E+00	1.84E-03	5.43E-04	2.20E-04
S2	53.01	17.81	9.83	-1.81E-04	1.63E-04	1.00E-06	2.03E-03	7.07E-04	2.19E-04
S3	52.99	17.82	9.79	1.80E-04	-1.62E-04	-1.00E-06	1.66E-03	3.81E-04	2.20E-04
S4	52.94	17.82	9.81	-1.00E-06	1.00E-06	0.00E+00	1.85E-03	5.45E-04	2.19E-04
Total Δv (km/sec):				Lambert=			Simulation=		
				9.83E-04			1.94E-02		

Table 7: Position Error and Δv with Iteration

$P1$	Δx	Δy	Δz	Δvx	Δvy	Δvz	Total Δv
S1	-0.01	-1.50	-0.06	2.16E-03	1.74E-03	2.21E-04	2.79E-03
S2	0.00	-1.52	-0.05	2.35E-03	1.58E-03	2.20E-04	2.84E-03
S3	0.02	-1.48	-0.05	1.98E-03	1.90E-03	2.21E-04	2.76E-03
S4	-0.01	-1.50	-0.02	2.17E-03	1.74E-03	2.20E-04	2.79E-03
$P2$							
S1	0.04	0.00	0.01	8.87E-04	4.89E-04	2.91E-04	1.05E-03
S2	-0.04	0.01	-0.01	1.07E-03	6.51E-04	2.91E-04	1.29E-03
S3	-0.02	0.00	0.03	7.01E-04	3.26E-04	2.92E-04	8.27E-04
S4	0.02	0.01	0.00	8.88E-04	4.90E-04	2.92E-04	1.06E-03

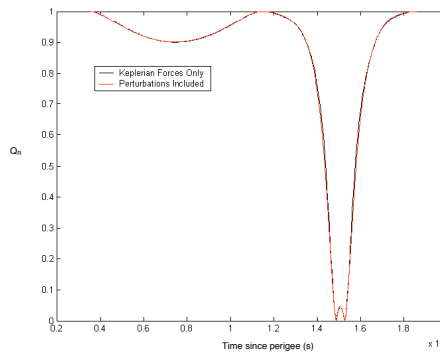


Figure 11: Quality Factor Comparison of Simulation Results

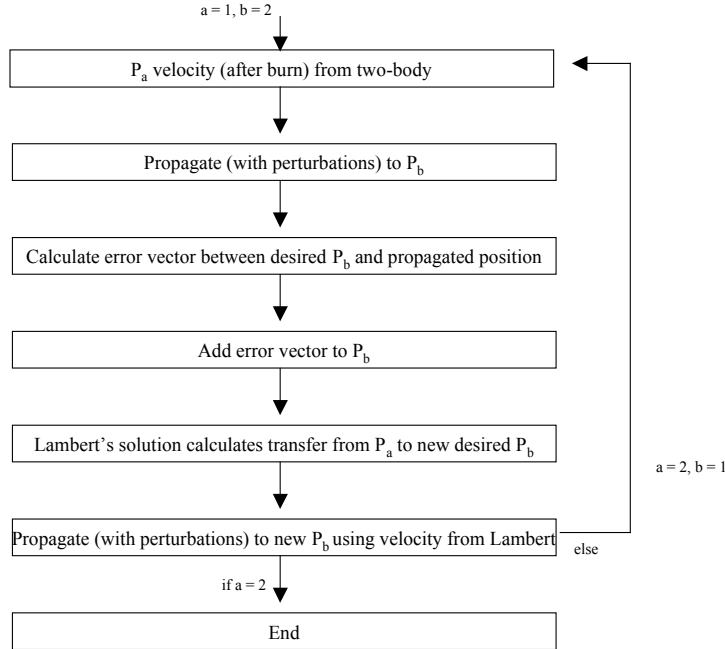


Figure 12. Iteration of Simulator

To correct the position error, the simulator is run given the two-body conditions for the transit from P_1 to P_2 . The position error between the simulator results and P_2 is calculated. Lambert's method is used to solve for the Δv 's needed to go from P_1 to locations that are offset from P_2 by the found error vector. The simulator is then reset to the initial conditions and the Δv 's calculated using the error vector are added and the formation is simulated to P_2 . The process is repeated for the transit from P_2 back to P_1 . Comparing Table 7 with Table 6 one can see the reduction in the position error results in the required Δv 's being decreased. Figure 12 is a diagram of the simulator iteration process. It might be beneficial to repeat this process to see if the position error could be reduced even more and thereby further reduce the Δv 's. However, the savings will not be nearly as significant for additional iterations.

In this analysis, the simulator is used as a post-processing step because of the computational time required for a single propagation. There is a substantial increase in the required amount of fuel, which must be taken into account during mission design. The above iteration scheme returns the satellites to approximately the same location each orbit. A summary of the perturbation analysis results is provided in Table 5.

The two-body results required very little fuel because spacecraft were on transfer orbits that follow an orbit with the same force model. The simulation results had satellites that were influenced by perturbing forces but attempted to follow an orbit propagated without these forces. Therefore, we hypothesized a significant reduction in fuel use could be achieved if the T-frame orbit was propagated using the same perturbing forces as were used to propagate the satellites.

To determine how much the fuel required could be reduced, we used a Simplified Deep Space Generalized Perturbations (SDP4) function of the SGP library²¹ to propagate both the T-frame and the satellites for our baseline solution. The results are presented in Table 5. There is an increase in the amount of fuel required because of the perturbing forces, but the amount of fuel is now a factor of 2.5 greater than that required by the baseline solution. We expect further improvement will be possible through use of SDP4 during optimization.

VIII. Conclusions and Future Work

Hierarchical and particle swarm optimization methods were applied to design a four-satellite tetrahedral formation in an elliptical geocentric orbit. As a compromise between purely natural and continuously controlled designs, this paper investigates multi-impulse formation designs where low-magnitude impulses are applied at specific orbital stations to maximize formation quality over a full orbit. We have studied a variety of dual-impulse designs applicable to the MMS mission, presuming perfect geometry at impulse application sites. We introduced a delay parameter to account for disturbances to the magnetic field following thruster use. For all test cases, a single-orbit solution was demonstrated superior to multi-orbit solutions given our Lambert-based impulse computation strategy. Alternative designs with perfect geometry away from impulse application sites were studied. Although the

integrated quality factor is lower when migrating the perfect geometry site away from impulse application stations, this result is not conclusive because it searches over a single perfect assembly site rather than constraining two sites to be perfect (as were the cases with perfect geometry at the two impulse sites). Although attitude has not yet been optimized, a “reconfiguration” study was performed where satellite were able to change tetrahedron vertices between impulse stations. Results showed a conflict between optimizing for fuel versus quality factor, suggesting a compromise solution might be possible should tetrahedron attitude also be optimized.

Hierarchical optimization provides a structured way to uniformly search or focus efforts on a specific part of the design vector space when the nature of local minima is known to some extent. However, to obtain accurate results without knowledge of minima region location or size, the search-space must often be refined such that large problems are infeasible to optimize. Although multiple iterations are required given its stochastic nature, PSO scales more readily to large optimization problems without the same computational penalty. In terms of solution quality, both optimization methods find similar solutions that are comparable in cost, utilizing multiple PSO trials improve statistical completeness.

A variety of different design strategies were presented in this paper. Although the choice of which option is best for a given mission is beyond the scope of this work, the PSO software can be expanded to handle multiple objectives through determination of the Pareto frontier. This information would give the mission designer a set of candidate solutions with different relative weights without repeated runs of each optimization tool.

Preliminary analyses have shown the error due to perturbations is nontrivial, and that although we can modify Δv application to maintain high quality factor, Δv magnitude increases by up to two orders of magnitude, suggesting alternative solutions may be optimal given realistic perturbations. Although it is not feasible to plug a full simulation into the optimizer due to computational complexity issues, the post-processing step of iterating the use of the simulator and Lambert’s method has reduced the error. Propagating the T-frame further decreased perturbation-related error, suggesting the future inclusion of the computationally efficient SDP4 during optimization.

Acknowledgments

The authors would like to thank Daniel Chavez Clemente for his development of the hierarchical optimization algorithm and software as well as his work on natural and VRB MMS formation designs We also thank Rob Sanner and Liam Healy for their development and assistance with the simulation and SGP software, and Steve Hughes and others in the GSFC Flight Dynamics group for their invaluable feedback. This work was partially supported under NASA GSFC Grant NNG04GA64A.

References

- ¹ Conkey, D., Dell, G., Good, S., and Bristow, J., “EO-1 formation Flying Using Autocon™”, *Proceedings of the IEEE Aerospace Conference*, Vol. 7, 2000, pp. 55-61.
- ² DeCou, A. B., “Orbital Station-Keeping for Multiple Spacecraft Interferometry,” *Journal of the Astronautical Sciences*, Vol. 39, No. 3, July-September 1991.
- ³ Hadaegh, F. Y., Lu, W.-M., and Wang, P. K. C., “Adaptive Control of Formation Flying Spacecraft for Interferometry,” IFAC, 1998.
- ⁴ Siegel, A., and Blandino, J., “Propulsion Requirements and Options for Astronomical Imaging Formations in Earth Orbit,” *Proceedings of the 39th AIAA/ASME/SAE/ASEE Joint Propulsion Conference*, Huntsville, Alabama, July 2003 (AIAA 2003-4577).
- ⁵ Vassar, R H; Sherwood, R B, “Formation keeping for a pair of satellites in a circular orbit”, *Journal of Guidance, Control, and Dynamics*, Vol. 8, Mar.-Apr. 1985, pp. 235-242.
- ⁶ Ren, W., and Beard, R., “Virtual Structure Based Spacecraft Formation Control with Formation Feedback,” *Proceedings of the AIAA Guidance, Navigation, and Control Conference*, Monterey, California, August 2002 (AIAA 2002-4963).
- ⁷ Campbell, M., and Schetter, T., “Comparison of Multiple Agent-Based Organizations for Satellite Constellations,” *Journal of Spacecraft and Rockets*, Vol. 39, No. 2, pp. 274-282, Mar.-Apr. 2002.
- ⁸ Penneçot, Y., Atkins, E., and Sanner, R., "Intelligent Spacecraft Formation Management and Path Planning," *Proceedings of the AIAA Aerospace Sciences Conference*, Reno, Nevada, January 2002 (AIAA 2002-1072).
- ⁹ Chavez-Clemente, D. and Atkins, E., “Optimization of Tetrahedral Satellite Formations,” *AIAA Journal of Spacecraft and Rockets*, vol. 42, no. 5, July-August 2005, pp. 699-710.
- ¹⁰ Curtis, S., “The Magnetospheric Multiscale Mission...Resolving Fundamental Processes in Space Plasmas”, NASA Technical Memorandum, NASA/GSFC, 2000.
- ¹¹ Curtis, S., Petruzzo, C., Clark, P., and Peterson, A., “*The Magnetospheric Multi-Scale Mission: An Electronically Tethered Constellation Of Four Spacecraft*”, IAF Conference, Pisa, Italy, Feb 2003.
- ¹² Hughes, S. P., “Formation Tetrahedron Design for Phase I of the Magnetospheric Multiscale Mission,” *Proc. of the Flight Mechanics Symposium*, NASA GSFC, October 2003.

- ¹³ Hughes, S. P., “Orbit Design for Phase I and II of the Magnetospheric Multiscale Mission”, *Proc. AAS 27th Rocky Mountain Guidance and Control Conference*, Breckenridge, Colorado, February 2004.
- ¹⁴ Robert, P., Roux, A., Harvey, C., Dunlop, M., Daly, P., and Glassmeier, K.-H., “Tetrahedron Geometric Factors,” in *Analysis Methods for Multi-Spacecraft Data* (edited by G. Paschmann and P. W. Daly), chap. 13, no. SR-001 in ISSI Scientific Reports, ESA Publ. Div., Noordwijk, Netherlands, 1998, pp. 323–348.
- ¹⁵ Eberhart, R. C. and Kennedy, J., “A New Optimizer Using Particle Swarm Theory,” *Proceedings of the Sixth International Symposium on Micromachine and Human Science*, Nagoya, Japan. p. 39-43, 1995
- ¹⁶ He, S., Prempain, E., and Wu, Q.H., “An Improved Particle Swarm Optimizer For Mechanical Design Optimization Problems,” *Engineering Optimization*, Vol. 36, No. 5, October 2004. p. 585–605.
- ¹⁷ Venter, G. and Sobieszczanski-Sobieski, J., “Multidisciplinary Optimization of a Transport Aircraft Wing Using Particle Swarm Optimization,” *9th AIAA/ISSMO Symposium on Multidisciplinary Analysis and Optimization*, Atlanta, Georgia, Sep. 4-6, 2002.
- ¹⁸ Guibout, V. M. & Scheeres, D. J., “Spacecraft Formation Dynamics and Design”, *Proceedings of the AIAA Guidance, Navigation and Control Conference and Exhibit*, Providence, Rhode Island, August 2004, (AIAA 2004 – 4736)
- ¹⁹ Hoskins, Aaron B. and Atkins, Ella M., “Formation Attitude Optimization with a Multi-Impulse Design”, *to appear at the NASA Goddard Flight Mechanics Symposium, Greenbelt, MD, October 2005*.
- ²⁰ Sanner, R. M., “SATCON Distribute Satellite Formation Simulation and Control Code,” Space Systems Lab Technical Report (in progress), Aerospace Engineering Department, University of Maryland, College Park, Maryland.
- ²¹ Hoots, Felix R. and Roehrich, Ronald L., “SPACETRACK REPORT NO. 3: Models for Propagation of NORAD Element Sets”, December 1980. (<http://celestrak.com/NORAD/documentation/spacetrk.pdf>).

Appendix: Multiple Orbit Data

Table A1: Multi-Orbit Dual-Impulse Solution Summary

Input:		Soln:						Stats:						
Test	Cost	D	Orb	Δv	v_c	$\tilde{\omega}_{true}$	V_x	V_y	V_z	$\Delta v/Orb$	Qdt/Orb	T_{obs}/Orb	$T_{obs} \%$	Cost
7	Qdt	0	2	6.06	3.3E-03	0.93	-9842.1	-9994.0	9638.7	2.6E+00	130724.8	144750	96.0%	-2.61E+05
8	Qdt	1hr	2	6.06	3.3E-03	0.93	-9842.1	-9994.0	9638.7	2.6E+00	126728.0	140750	93.3%	-2.53E+05
9	$\Delta v/T_{obs}$	0	2	5.63	1.7E-02	0.89	-9755.6	-9122.2	9467.4	6.5E-04	86586.7	99500	66.0%	6.54E-09
10	$\Delta v/T_{obs}$	1hr	2	0.16	5.2E-01	0.09	-9783.3	-9467.9	6907.4	3.4E-04	56017.8	65250	43.3%	5.20E-09
11	Both	0	2	5.60	8.1E-02	0.88	-9688.1	-9893.6	9503.9	6.2E-04	87537.2	102000	67.6%	-1.67E+05
12	Both	1hr	2	5.60	8.0E-02	0.88	-9708.8	-9870.0	9526.3	6.2E-04	83758.6	98250	65.2%	-1.59E+05
13	Qdt	0	3	6.28	5.0E-02	1.01	-9827.0	-9440.7	-9333	4.1E+00	117833.7	141667	94.0%	-3.54E+05
14	Qdt	1hr	3	6.28	9.7E-02	1.01	-9564.3	-9520.1	-9823	4.4E+00	116094.9	139833	92.7%	-3.48E+05
15	$\Delta v/T_{obs}$	0	3	0.17	2.5E+00	1.61	-9479.8	-8044.1	-7510	3.1E-04	19155.4	20000	13.3%	1.57E-08
16	$\Delta v/T_{obs}$	1hr	3	0.01	2.5E+00	1.11	-8445.2	-5033.7	-6958	2.7E-04	15437.7	16167	10.7%	1.69E-08
17	Both	0	3	5.19	9.3E-02	3.10	9035.8	-4085.9	7508.7	6.0E-04	26784.4	30500	20.2%	-5.47E+04
18	Both	1hr	3	0.01	2.5E+00	1.11	-8445.2	-5033.7	-6958	2.7E-04	15437.7	16167	10.7%	-2.43E+04
19	Qdt	0	4	6.27	1.3E-01	0.89	-8532.2	-8151.4	8909.9	4.4E+00	90197.9	107625	71.4%	-3.61E+05
20	Qdt	1hr	4	6.27	1.3E-01	0.89	-8532.2	-8151.4	8909.9	4.4E+00	88199.5	105625	70.0%	-3.53E+05
21	$\Delta v/T_{obs}$	0	4	0.14	2.5E+00	1.46	-8289.2	-9088.2	-8301	1.9E-04	15139.6	16250	10.8%	1.18E-08
22	$\Delta v/T_{obs}$	1hr	4	0.18	6.9E-01	0.13	-9928.7	-8524.1	856.3	2.0E-04	11731.9	12250	8.1%	1.62E-08
23	Both	0	4	5.29	3.8E-02	0.65	-8389.9	-8213.9	-399.1	4.5E-04	18888.9	20875	13.8%	-4.77E+04
24	Both	1hr	4	0.03	6.7E-01	0.10	-9755.1	-7481.4	-9797	1.8E-04	12854.2	13500	9.0%	-3.42E+04